

Coherent scattering 2D cooling in levitated cavity optomechanics

Marko Toroš,¹ Uroš Delić,² Fagin Hales,¹ and Tania S. Monteiro¹

¹*Department of Physics and Astronomy, University College London, Gower Street, WC1E 6BT London, United Kingdom.*

²*Vienna Center for Quantum Science and Technology, Faculty of Physics, University of Vienna, A-1090 Vienna, Austria.*

The strong light-matter optomechanical coupling offered by Coherent Scattering (CS) set-ups have allowed the experimental realisation of quantum ground state cavity cooling of the axial motion of a levitated nanoparticle [U. Delić et al., *Science* 367, 892 (2020)]. An appealing milestone is now quantum 2D cooling of the full in-plane motion, in any direction in the transverse plane. By a simple adjustment of the trap polarisation, one obtains two nearly equivalent modes, with similar frequencies $\omega_x \sim \omega_y$ and optomechanical couplings $g_x \simeq g_y$ – in this experimental configuration we identify an optimal trap ellipticity, nanosphere size and cavity linewidth which allows for efficient 2D cooling. Moreover, we find that 2D cooling to occupancies $n_x + n_y \lesssim 1$ at moderate vacuum (10^{-6} mbar) is possible in a “Goldilocks” zone bounded by $\sqrt{\kappa\Gamma/4} \lesssim g_x, g_y \lesssim |\omega_x - \omega_y| \lesssim \kappa$, where one balances the need to suppress dark modes whilst avoiding far-detuning of either mode or low cooperativities, and κ (Γ) is the cavity decay rate (motional heating rate). With strong-coupling regimes $g_x, g_y \gtrsim \kappa$ in view one must consider the genuine three-way hybridisation between x, y and the cavity light mode resulting in hybridized bright/dark modes. Finally, we show that bright/dark modes in the levitated set-up have a simple geometrical interpretation, related by rotations in the transverse plane, with implications for directional sensing.

I. INTRODUCTION

The coupling between light and matter has led to major milestones in physics, from the Michelson-Morley experiment [1] to the detection of gravitational waves by the LIGO collaboration [2]. The basic scheme relies on the light acting as a probe – offering exceptional sensitivities – which is now routinely done in state-of-the-art optomechanical systems with high-quality mirrors. The latter are themselves interesting systems and have led to the field of cavity optomechanics [3]. A mirror with a motional degree of freedom cooled to its ground state is of particular interest as it becomes a quantum sensor and can thus be used as a detector of weak forces and as a probe of the quantum-to-classical transition [4].

On the other hand quantum features of an object in all three spatial dimensions – with applications ranging from quantum foundations to directional sensing – can be explored using an optically levitated nanoparticle [5–9]. Initial experimental efforts have been hindered by technical difficulties of stable trapping in high vacuum [10, 11] and several implementations have been considered such as hybrid tweezer-cavity traps [12, 13], electro-optical traps [14, 15], and trapping in the near field of a photonic crystal [16].

Recently, a 3D coherent scattering (CS) setup was introduced to levitated cavity optomechanics [18, 19] using methods adapted from atomic physics [20–24]. In contrast to experiments that consider dispersive coupling, here the cavity is driven solely by the dipole radiation of the optically trapped silica particle. Due to the tight focus of the optical tweezer this scheme yields unprecedentedly high optomechanical coupling rates, which subsequently enabled ground-state cooling of the motion along the cavity axis and thus opened the door to quantum levitated optomechanics [17].

For the purpose of prolonging available free fall ex-

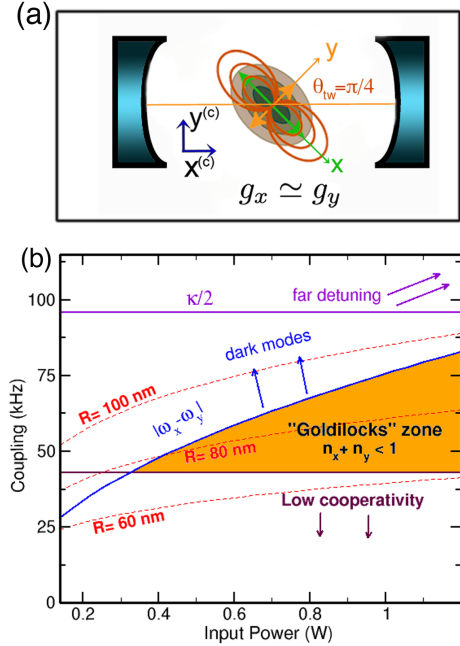


Figure 1. **(a)** Schematic of coherent-scattering experiments: an adjustment of the tweezer polarisation ($\theta_{tw} = \pi/4, 3\pi/4$) yields two equivalently coupled x, y mechanical modes, $|g_x| \simeq |g_y| \simeq g$. **(b)** We find there is a “Goldilocks” region (orange) for 2D ground state cooling i.e. $n_x + n_y \lesssim 1$, illustrated for the set-up of [17] but with $\theta_{tw} = \pi/4$. The optimal region lies below the blue curve to avoid the formation of decoupled dark modes (i.e., $|\omega_x - \omega_y| \gtrsim g$), is bounded from above by the constraint to avoid far-detuning ($\kappa \gtrsim |\omega_x - \omega_y|$), and from below by the regime of weak quantum cooperativities (i.e., $C = 4g^2/(\kappa\gamma n_B) \gtrsim 1$, where γ (n_B) is the gas damping (mean thermal occupancy)). Red lines correspond to different particle sizes and indicate $R \sim 80$ nm is optimal.

periment times [25], an important future milestone for the coherent scattering setup is the simultaneous ground state cooling of all three translational degrees of freedom. Here we focus on the motions in the tweezer transverse plane (x - y plane) which both have the standard position-position type coupling to the cavity mode. Both have similar frequencies $\omega_x \approx \omega_y$ and by means of a suitable adjustment, $g_x \simeq g_y \simeq g$, where $g \equiv (g_x + g_y)/2$. On the other hand, the frequency of the z -motion is typically $\omega_z \ll \omega_{x,y}$ such that it is well removed from the optomechanical resonance, but can be cooled using feedback cooling [26].

In this work we investigate 2D cooling regimes by exploiting the recently developed 3D coherent scattering theory [27]. We optimize 2D cooling with respect to particle size, trap frequencies, tweezer polarization orientation, as well as detuning between the tweezer frequency and cavity resonance. For readily achieved experimental pressures of $p = 10^{-6}$ mbar we identify a ‘‘Goldilocks’’ region $\sqrt{\kappa\Gamma}/4 \lesssim g_x, g_y \lesssim |\omega_x - \omega_y| \lesssim \kappa$, where κ (Γ) is the cavity decay rate (heating rate). This set of requirements minimizes the formation of decoupled dark modes and optimizes 2D cooling for $|\omega_x - \omega_y| \sim \kappa/2$ by using a particle of radius ~ 80 nm. While bright/dark modes have been previously investigated in optomechanical systems [28] in the levitated system they have a geometric interpretation in terms of the rotation of the x, y axes of the oscillator, with potential implications for directional sensing. The importance of non-degenerate mechanical frequencies $\omega_x \neq \omega_y$ for successful 2D cooling is a well known fact in experiments with trapped ions and atoms [23, 29].

This work is organized in the following way. We start by reviewing the coherent scattering setup and introducing the relevant experimental parameters (Sec. II). We then illustrate how mechanical modes hybridize with the optical mode, resulting in the formation of bright/dark modes and 3-way mixing. In particular, we show how dark modes distort the relation between the displacement and heterodyne spectra, making in general thermometry and sensing non-trivial (Sec. III). We tackle this problem by adjusting the tweezer polarization in such a way to symmetrize the optomechanical couplings (i.e., $g_x \sim g_y$), which simplifies the relations between displacement/heterodyne spectra to a form resembling the familiar ones from the usual 1D cavity-optomechanics. In the central part we give a detailed analysis of 2D cooling and discuss how to perform thermometry (Sec. IV) as well as identify the best parameters for 2D cooling by numerically scanning the experimental parameters (Sec. V). We conclude by laying down a path for 3D motional ground state cooling in the levitated optomechanics – in particular, how 2D cavity-optomechanical cooling can be combined with feedback cooling to achieve the 3D motional ground state of the optically levitated system (Sec. VI).

II. EXPERIMENTAL SETUP

We consider the 3D coherent scattering setup illustrated in Fig. 1(a). The nanoparticle is trapped in an optical tweezer and positioned inside an optical cavity – the cavity is driven entirely by the tweezer light scattered off the nanoparticle, namely, coherent scattering with a pattern shown in Fig. 1(a). Such a scheme offers unique versatility with respect to the customary cavity optomechanical system, since the nanoparticle can be placed at any point inside the cavity by displacing the tweezer trap. Here we will consider the case when the nanoparticle is close to a *cavity node* $x_0^{(c)} \sim \lambda/4$ (λ : laser wavelength), where the strongest coupling to the nanoparticle x and y motions is achieved. In addition, deleterious effects of cavity photon scattering and recoil heating are minimal.

Linearisation of the effective potentials in the CS setups [18, 19] has shown that :

$$g_x = -E_d k \sin(\theta_{tw}) x_{zpf}, \quad g_y = -E_d k \cos(\theta_{tw}) y_{zpf} \quad (1)$$

where we have defined the driving as $E_d = \frac{\alpha \epsilon_c \epsilon_{tw} \sin(\theta)}{2\hbar}$, $\alpha = 3\epsilon_0 V_s \frac{\epsilon_R - 1}{\epsilon_R + 2}$ (ϵ_0 is the permittivity of free space, V_s is the volume of the nanoparticle, ϵ_R is the relative dielectric permittivity), $\epsilon_c = \sqrt{\frac{\hbar \omega_c}{2\epsilon_0 V_c}}$ (ω_c is the cavity frequency, V_c is the cavity volume), and $\epsilon_{tw} = \sqrt{\frac{4P_{tw}}{w_x w_y \pi \epsilon_0 c}}$ (P_{tw} is the tweezer power, and w_x, w_y is the waist of the Gaussian beam along the x or y -axis respectively).

The angle θ_{tw} between the tweezer polarization axis (y -axis) and the cavity symmetry axis ($x^{(c)}$ -axis) can be arbitrarily set to tune coupling rates g_x and g_y . Motional 1D ground state cooling (of a single mechanical degree of freedom) along $x^{(c)}$ has been recently achieved by setting $\theta_{tw} \sim \pi/2$. In this case the *tweezer-based* coordinates (x, y) and the *cavity-based* coordinates ($x^{(c)}, y^{(c)}$) identify the same point in the 2D plane orthogonal to the tweezer symmetry axis, z .

However, one obtains $g_x \approx g_y$ for $\theta_{tw} = \pi/4$ and that is the regime we consider for 2D cooling. The motion along the z -axis is effectively decoupled (we have $\omega_z \ll \omega_x, \omega_y$) and will be omitted in the following to simplify the presentation (but has been taken into account when calculating numerically the power spectral densities (PSDs) according to the full 3D cooling theory of [27]).

III. BRIGHT/DARK MODES

Avoided crossings are ubiquitous in physics. For example, two classical (or quantum) modes, say \hat{x} and \hat{y} , approaching an energy degeneracy are universally described by a Hamiltonian represented in terms of Pauli matrices:

$$\frac{\hat{V}_{int}}{\hbar} = \frac{1}{2} \begin{bmatrix} \hat{x} & \hat{y} \end{bmatrix} [(\omega_x - \omega_y)\hat{\sigma}_z + 2g\hat{\sigma}_x] \begin{bmatrix} \hat{x} \\ \hat{y} \end{bmatrix}, \quad (2)$$

where g is the coupling. At the degeneracy, $\omega_x = \omega_y$, the modes of the system correspond to the eigenmodes of $\hat{\sigma}_x$

which are given by $\hat{x} \pm \hat{y}$. Here the normal modes are maximally hybridized and the corresponding frequencies perturbed by $\pm g$.

In regimes of negligible-dissipation $g \gg \kappa, \gamma$, the usual optomechanical interaction corresponds to a two-mode avoided crossing. The two-mode crossing was demonstrated experimentally in optomechanics [30] where it was observed that the cavity light mode and mechanical modes were hybridized with a splitting $2g$, and more recently investigated using levitated nanoparticles [31].

In the present case, we have a *three-mode* avoided crossing. These are less frequently encountered, but may be discussed in a similar way. Two mechanical modes, \hat{x} and \hat{y} , are coupled to the optical mode, \hat{Z}_L , according to the usual position-position form (see Sec. IV for more details):

$$\frac{\hat{V}_{\text{int}}}{\hbar} = g_x \hat{x} \hat{Z}_L + g_y \hat{y} \hat{Z}_L, \quad (3)$$

Representing the modes as a vector, $[\hat{x} \hat{Z}_L \hat{y}]^\top$ and Eq. (3) in matrix form we write:

$$\frac{\hat{V}_{\text{int}}}{\hbar} = \frac{1}{4} [\hat{x} \hat{Z}_L \hat{y}] \begin{bmatrix} \omega_x & 2g_x & 0 \\ 2g_x & -\Delta & 2g_y \\ 0 & 2g_y & \omega_y \end{bmatrix} \begin{bmatrix} \hat{x} \\ \hat{Z}_L \\ \hat{y} \end{bmatrix} \quad (4)$$

where we have also included the two mechanical frequencies, ω_x, ω_y , and the detuning, $-\Delta$.

We first consider equal couplings $g_x = g_y \equiv g$, and set $-\Delta = (\omega_x + \omega_y)/2$. Neglecting the term $\frac{1}{4} \frac{\omega_x + \omega_y}{2} \mathbb{I}$, where \mathbb{I} is the identity, we write:

$$\frac{\hat{V}_{\text{int}}}{\hbar} = \frac{1}{4} [\hat{x} \hat{Z}_L \hat{y}] \left[(\omega_x - \omega_y) \hat{S}_z + 2\sqrt{2}g \hat{S}_x \right] \begin{bmatrix} \hat{x} \\ \hat{Z}_L \\ \hat{y} \end{bmatrix}, \quad (5)$$

where now \hat{S}_x, \hat{S}_z are spin 1 matrices (divided by \hbar). The associated anticrossing has an enhanced width of $2\sqrt{2}g$.

For the degenerate case, $\omega_x = \omega_y$, the eigenmodes are simply the textbook eigenvectors of the \hat{S}_x matrix: in that case, there are two *three-way* hybridised ‘‘bright’’ eigenmodes (\hat{B}^\pm) with eigenvalues $\pm\sqrt{2}g$, and a *two-way* hybridised ‘‘dark’’ eigenmode (\hat{D}) with eigenvalue zero:

$$\hat{B}^\pm = \frac{1}{2} [\hat{x} + \hat{y} \pm \sqrt{2} \hat{Z}_L], \quad (6)$$

$$\hat{D} = \frac{1}{\sqrt{2}} [\hat{x} - \hat{y}]. \quad (7)$$

While the pedagogic Eq. (5) was not used to compute the realistic system eigenmodes, it illustrates the significance of lifting the frequency degeneracy: $\omega_x \neq \omega_y$ introduces a \hat{S}_z component that mixes the bright dark modes \hat{D}, \hat{B}^\pm . The case $g_x \neq g_y$ (but $\omega_x \sim \omega_y$) does not eliminate the bright-dark mode structure: it simply alters the dark eigenvectors at the centre of the crossing to

$$\hat{D} = \frac{1}{\epsilon} [g_y \hat{x} - g_x \hat{y}] \quad (8)$$

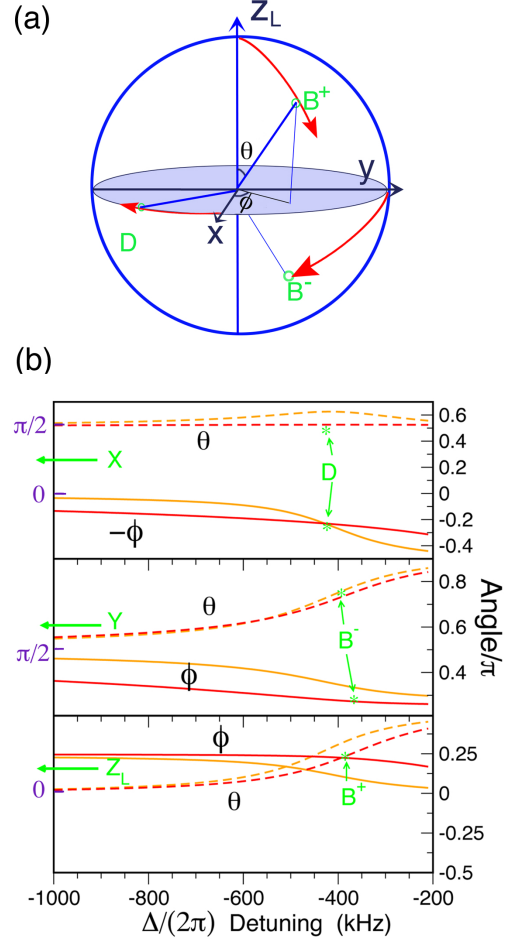


Figure 2. (a) Trajectories of idealised bright and dark modes, represented on a Bloch sphere where the vector of unit length $\hat{\mathbf{n}} = [\hat{x}, \hat{y}, \hat{Z}_L] \doteq [\theta, \phi]$ represents a mode at a given Δ . As $\Delta \rightarrow -(\omega_x + \omega_y)/2$ (the centre of the crossing), the ideal dark mode rotates on the ‘equator’ from $\phi = 0$ (at $\Delta = -\infty$) through an angle $\phi = -\pi/4$ (at $\Delta \rightarrow -(\omega_x + \omega_y)/2$), thus evolves from the \hat{x} mode to \hat{D} . The ‘bright’ modes \hat{Z}_L (\hat{y}) rotate to B^+ (B^-). (b) Compares the trajectories using solutions of the classical equations of motion and for realistic parameters: either the elliptical trap (with $\delta\omega = |\omega_x - \omega_y|$ of order 16% of $\omega_{x,y}$) and parameters of the quantum ground state cooling experiments in [17] (orange lines), or a more circular trap where frequencies differ by about 3.5% (red lines). The near circular trap follows the idealised dark/bright modes illustrated in (a), while for the elliptical trap the ‘dark’ mode still rotates by $\phi \simeq -\pi/4$ but does not remain on the equator, thus mixes with the optical mode.

(which is still a dark mode with eigenvalue 0) while the bright modes are $\hat{B}^\pm = \frac{1}{\sqrt{2}} [\frac{g_x}{\epsilon} \hat{x} + \frac{g_y}{\epsilon} \hat{y} \pm \hat{Z}_L]$ (with eigenvalues $\epsilon = \pm \sqrt{g_x^2 + g_y^2}$). However, we see that as $g_y \rightarrow 0$, $\hat{D} \rightarrow \hat{y}$. This is the quasi-1D dynamics analysed in [27] (using $\theta_{tw} = 85$ degrees). In this limit, the \hat{y} mode is ‘‘dark’’ simply because it is very weakly coupled.

The true eigenmodes of the coherent scattering set-up, for arbitrary Δ , were computed numerically from the equations of motion of the system. The Hamiltonian for the reduced 2D case can be put in the following form:

$$\begin{aligned} \frac{\hat{H}}{\hbar} = & -\frac{\Delta}{4}(\hat{Z}_L^2 + \hat{P}_L^2) + \frac{\omega_x}{4}(\hat{x}^2 + \hat{p}_x^2) \\ & + \frac{\omega_y}{4}(\hat{y}^2 + \hat{p}_y^2) + g_x \hat{x} \hat{Z}_L + g_y \hat{y} \hat{Z}_L, \end{aligned} \quad (9)$$

where ω_x , ω_y are the frequencies of the two harmonic motions, \hat{x} , \hat{y} (\hat{p}_x , \hat{p}_y) are the the position (momentum) observables, g_x , g_y denote the optomechanical couplings (see Eq. (1)), and \hat{Z}_L (\hat{P}_L) denote the amplitude (phase) quadrature of the intracavity field.

The resulting equations of motion, including dissipation and Gaussian noise baths acting on each mode, yield a set of linear coupled equations which are represented in the well-known form:

$$\dot{\mathbf{X}} = \mathbf{A}\mathbf{X} + \sqrt{\Gamma}\mathbf{X}_{\text{in}}(t) \quad (10)$$

where \mathbf{A} is a drift matrix that includes dissipative terms and j th element of the vector $(\mathbf{A}\mathbf{X})^{(j)} = \frac{1}{i\hbar}[\mathbf{X}^{(j)}, \hat{H}] - \frac{1}{2}(\mathbf{\Gamma}\mathbf{X})^{(j)}$. For our discussion we neglect the z -motion (but it is included in quantum numerics), so can consider \mathbf{A} as a 6×6 matrix. \mathbf{X} is the vector of the mechanical and optical modes, $\mathbf{X} = (\hat{x}, \hat{p}_x, \hat{y}, \hat{p}_y, \hat{Z}_L, \hat{P}_L)^T$, $\sqrt{\Gamma}$ represents the diagonal matrix of damping coefficients while $\mathbf{X}_{\text{in}}(t)$ represents the Gaussian noises (gas collisions and optical shot noises).

To obtain the classical normal modes and frequencies of the system, we calculated the eigenvalues and eigenvectors of \mathbf{A} as a function of the optical detuning Δ . It was sufficient for our classical analysis to consider the case with dissipative terms set to zero ($\sqrt{\Gamma} = 0$).

Such eigenmodes can be represented as unit vectors in the space spanned by the tweezer modes \hat{x} , \hat{y} , and \hat{Z}_L , i.e., as spherical polar angles on a Bloch sphere (see Fig. (2) (a)). As the detuning is varied from $\Delta = -\infty$ to $\Delta \sim 0$ we represented the resulting trajectory traced by each eigenmode using the corresponding spherical polar angles – Fig. 2(b) plots the trajectories as a function of detuning Δ for two realistic scenarios. In the first case (orange lines) we employ the experimental parameters of [17] and thus a more elliptical tweezer trap $w_x = 0.6\mu\text{m}$, $w_y = 0.705\mu\text{m}$ where tweezer frequencies differ by about 16%. In the second case (red lines) we set $w_x = 0.68\mu\text{m}$, so now the frequencies are near-degenerate (near circular trap) and differ by about 3.5%.

The plots indicate that the red lines remain close to the ‘dark/bright’ modes of Eq. (7). We see the dark mode simply rotates on the ‘equator’ ($\theta = \pi/2$), from $\phi = 0$ at $\Delta = -\infty$ through to $\phi = -\pi/4$ at the centre of the crossing where $-\Delta = \omega_x \simeq \omega_y$. For the elliptical trap of the experiment [17] however, the ‘dark’ mode (top panel) still rotates to $\phi = -\pi/4$ at the centre of the crossing but mixes appreciably with the optical mode ($\theta \simeq 0.6\pi$).

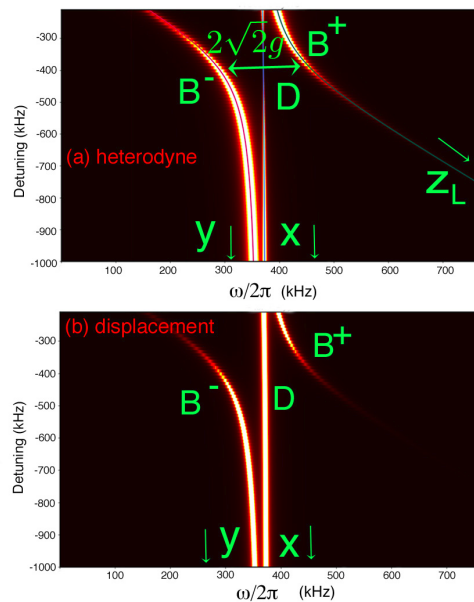


Figure 3. **(a)** Illustrates heterodyne PSD $S_{\text{het}}(\omega)$, in regimes where the \hat{x} , \hat{y} and optical modes hybridise to form bright (\hat{B}^{\pm}) and dark (\hat{D}) modes, i.e., where $g \gg |\omega_x - \omega_y|, \kappa, \gamma$. The solid lines overlaid are the classical modes. The central dark mode reaches near zero amplitude at the centre of the crossing. The bright modes show an avoided crossing of width enhanced by a factor of $\sqrt{2}$. **(b)** In contrast, the displacement PSD, $S_{xx}(\omega) + S_{yy}(\omega)$ show that both dark and bright modes are uncooled and remain hot.

The more general case of $g_x \neq g_y$ (and arbitrary detuning) does not eliminate the bright-dark mode structure. In contrast lifting the $\omega_x \sim \omega_y$ degeneracy has a pronounced effect – the bright/dark modes mix and very different trajectories are obtained. Ultimately this would lead to a decoupling to two independent level crossings, with the associated disadvantage that both modes might no longer be resonant simultaneously – this case depends on κ and is investigated below.

Fig. 3(a) illustrates the characteristics of a heterodyne PSD $S_{\text{het}}(\omega)$, in regimes of bright dark-modes, where $g \gg |\omega_x - \omega_y|, \kappa, \gamma$ so dissipation is very low. Specifically, the parameters are set close to experiment of [17] but with $\theta_{tw} = \pi/4$, $\kappa \rightarrow \kappa/10$ and $|\omega_x - \omega_y| \rightarrow |\omega_x - \omega_y|/4$. The figure illustrates the typical structure of a 3-level crossing with a coupling in the form of Eq. (4) (two degenerate modes \hat{x}, \hat{y} couple indirectly via a third). It illustrates however also the difficulty of the usual procedure for thermometry in optomechanics. Both modes are hot, and moreover the usual normalisation used to relate the heterodyne measured PSD to the underlying displacement spectra gives very poor results.

IV. 2D MOTION MODELING

The Hamiltonian of the system, Eq. (9) is a special case of the Hamiltonians discussed in [18, 27] where the nanoparticle equilibrium position was primarily determined by the gradient force ($\sim 70\text{nm}$ particles). Here we however consider also substantially larger particles ($\sim 100\text{nm}$) where the scattering force must be taken into account. In particular, the latter displaces the nanoparticle equilibrium position which leads to new couplings of \hat{x} and \hat{y} to the phase quadrature of light, \hat{P} (in addition, to the coupling to the amplitude quadrature, \hat{Y}). In Appendix A we show that the Hamiltonian can be transformed back to the form in Eq. (9) by introducing the rotated optical quadratures \hat{Z}_L (\hat{P}_L) with the rotation angle depending on the size of the nanoparticle. In short, all of the results from [18, 27] remain valid even when the scattering force is non-negligible (but still in the Rayleigh regime) as long as we formally replace \hat{Y}, \hat{P} with the rotated optical quadratures \hat{Z}_L, \hat{P}_L .

Here we are assuming that we operate at the cavity node, i.e., $\phi_{\text{tw}} = \pi/2$, where we ask the the following question: what is the optimal angle θ_{tw} between the tweezer polarization axis and the cavity symmetry axis for efficient 2D cooling? The latter controls the couplings g_x, g_y , and the most natural choice is given by $\theta_{\text{tw}} \sim \pi/4$ where $g_x \sim g_y$ – this maximizes the cooperativities of both the x and y motions. In addition, we have the freedom in choosing the detuning, Δ ($\Delta < 0$ is red-detuned) – in first instance this can be set to $-\Delta = (\omega_x + \omega_y)/2$. In particular, the perfectly degenerate case, $\omega_x = \omega_y$, where we have the exact relation $g_x = g_y$ seems the most natural configuration for 2D cooling – however, we will show this is not the case, and non-degenerate frequencies are necessary for efficient 2D cooling.

The 2D equations of motion $\dot{\mathbf{X}} = \mathbf{A}\mathbf{X}$ in Eq.(10), explicitly, are given by:

$$\dot{\hat{x}} = \omega_x \hat{p}_x, \quad \dot{\hat{p}}_x = -\omega_x \hat{x} - 2g_x \hat{Z}_L, \quad (11)$$

$$\dot{\hat{y}} = \omega_y \hat{p}_y, \quad \dot{\hat{p}}_y = -\omega_y \hat{y} - 2g_y \hat{Z}_L, \quad (12)$$

$$\dot{\hat{Z}}_L = -\Delta \hat{P}_L, \quad \dot{\hat{P}}_L = \Delta \hat{Z}_L - 2g_x \hat{x} - 2g_y \hat{y}, \quad (13)$$

where we have for simplicity of presentation omitted the non-conservative terms (damping terms and input noises). We have the optical quadratures, $\hat{Z}_L = \hat{a} + \hat{a}^\dagger$ and $\hat{P}_L = i(\hat{a}^\dagger - \hat{a})$, x mechanical quadratures, $\hat{x} = \hat{b}_x + \hat{b}_x^\dagger$ and $\hat{p}_x = i(\hat{b}_x^\dagger - \hat{b}_x)$, and the y mechanical quadratures, $\hat{y} = \hat{b}_y + \hat{b}_y^\dagger$ and $\hat{p}_y = i(\hat{b}_y^\dagger - \hat{b}_y)$. We transform Eqs. (11)-(13) to second order differential equations by eliminating the momenta, and express the resulting equations in Fourier space:

$$\hat{x}(\omega) = J_{xz}(\omega) \hat{Z}_L(\omega) + \tilde{x}_{\text{in}}(\omega), \quad (14)$$

$$\hat{y}(\omega) = J_{yz}(\omega) \hat{Z}_L(\omega) + \tilde{y}_{\text{in}}(\omega), \quad (15)$$

$$\hat{Z}_L(\omega) = J_{Zx}(\omega) \hat{x}(\omega) + J_{Zy}(\omega) \hat{y}(\omega) + \tilde{Z}_{L,\text{in}}(\omega), \quad (16)$$

which can be readily solved for $\hat{x}(\omega)$, $\hat{y}(\omega)$ and $\hat{Z}_L(\omega)$ (in terms of the input noises $\tilde{x}_{\text{in}}(\omega)$, $\tilde{y}_{\text{in}}(\omega)$ and $\tilde{Z}_{L,\text{in}}(\omega)$). The frequency dependent coupling coefficients are given by

$$J_{jz}(\omega) = 2g_j \chi_j(\omega), \quad (17)$$

$$J_{Zj}(\omega) = ig_j \eta(\omega), \quad (18)$$

where $j = x, y$, the susceptibilities are given by

$$\chi_j(\omega) = \frac{\omega_j}{-\omega^2 + \omega_j^2 - i\omega_j \gamma}, \quad (19)$$

$$\eta(\omega) = \frac{1}{-i(\omega + \Delta) + \frac{\kappa}{2}} - \frac{1}{i(-\omega + \Delta) + \frac{\kappa}{2}}, \quad (20)$$

and κ (γ) is the cavity decay rate (gas damping).

Eqs. (14)-(16) form a system of coupled equations: the solutions $\hat{x}(\omega)$, $\hat{y}(\omega)$, $\hat{a}(\omega)$ are function of the input noises $\tilde{x}_{\text{in}}(\omega)$, $\tilde{y}_{\text{in}}(\omega)$, $\tilde{a}_{\text{in}}(\omega)$. In addition to gas collisions and photon shot-noise we also include recoil heating in the model by adding additional terms to $\tilde{x}_{\text{in}}(\omega)$ and $\tilde{y}_{\text{in}}(\omega)$ [18, 32, 33]. The latter can become relevant even at pressure $p \sim 10^{-6}$ mbar when we scan over large values of the couplings $g_x, g_y \gtrsim 100\text{kHz}$ as we increase the size of the nanoparticle/laser power.

Closed form PSDs for $S_{xx}(\omega) = \langle |\hat{x}^{3\text{D}}(\omega)|^2 \rangle$ or $S_{yy}(\omega) = \langle |\hat{y}^{3\text{D}}(\omega)|^2 \rangle$ were calculated and thence phonon occupancies are related to the area under the PSD curve [34]:

$$n_j = \frac{1}{2\pi} \int_{-\infty}^{\infty} S_{jj}(\omega) d\omega - \frac{1}{2} \quad (21)$$

for $j = x, y$. We refer the reader to the full 3D analysis discussed in detail in [27] which reduces to the 2D case discussed here when the z -motion can be neglected.

Scattering force and optomechanical couplings

Eq. (9) on first sight appears to be a special case of the Hamiltonians discussed in [18, 27] where the nanoparticle equilibrium position was primarily determined by the gradient force ($\sim 70\text{nm}$ particles). Here we however consider also substantially larger particles ($\sim 100\text{nm}$) where the scattering force must be taken into account. In particular, the latter displaces the nanoparticle equilibrium position which leads to new couplings of \hat{x} and \hat{y} to the phase quadrature of light, \hat{P} (in addition, to the coupling to the amplitude quadrature, \hat{Y}). In Appendix A we show that the Hamiltonian can be transformed back to the form in Eq. (9) by introducing the rotated optical quadratures \hat{Z}_L (\hat{P}_L) with the rotation angle depending on the size of the nanoparticle. In short, all of the results from [18, 27] remain valid even when the scattering force is non-negligible (but still in the Rayleigh regime) as long as we formally replace \hat{Y}, \hat{P} with the rotated optical quadratures \hat{Z}_L, \hat{P}_L .

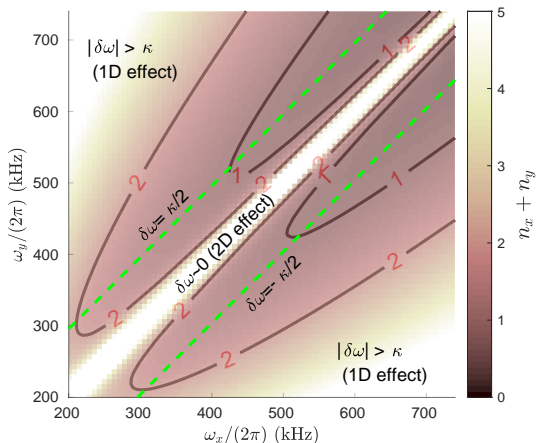


Figure 4. Numerical simulation of 2D phonon occupancy as a function of the tweezer frequencies ω_x and ω_y . The values are set as in [17] but $\theta = \pi/4$ but with variable tweezer waists along the x, y -axis. Cooling becomes ineffective in two regimes of $\delta\omega = |\omega_x - \omega_y|$: (i) when the trap is near circular and a decoupled dark mode is formed (diagonal white strip) or (ii) the frequency difference $\delta\omega$ is too large compared to the cavity decay rate κ (white regions in top left and bottom right corners). Cooling is optimal for intermediate frequency differences when $\delta\omega$ is close to $\kappa/2$.

V. 2D COOLING – NUMERICAL RESULTS

We define the mechanical 2D phonon occupancy as

$$\hat{n}^{(2D)} = \hat{n}_x + \hat{n}_y, \quad (22)$$

where $\hat{n}_x = \hat{b}_x^\dagger \hat{b}_x$ and $\hat{n}_y = \hat{b}_y^\dagger \hat{b}_y$. The latter will be calculated using Quantum Linear Theory (QLT) by numerically integrating the associated power spectral densities (PSDs), S_{xx} and S_{yy} (see Sec. IV). In particular, in the following we will consider the condition $\hat{n}^{(2D)} < 1$ as a threshold value for 2D motional ground state cooling. Alternatively we could have required the less restrictive conditions $\hat{n}_x, \hat{n}_y < 1$, i.e. the two motions are separately in the ground state (see Appendix B for a brief discussion how to quantify 2D cooling in the transverse x - y plane).

A. Optimal frequency difference

The first question we address is what is the optimal frequency difference, $\delta\omega = |\omega_x - \omega_y|$, in order to achieve the lowest combined phonon occupancy $\hat{n}^{(2D)}$. For concreteness we will consider the parameters from [17] (but now with $\theta = \pi/4$) and vary the two waists of the tweezer beam, w_x and w_y , to scan over the frequencies, ω_x, ω_y . We find that when $|\omega_x - \omega_y| > \kappa$ simultaneous cooling of the \hat{x} and \hat{y} modes becomes ineffective – we either cool x -motion or y -motion, but cannot cool both effectively.

More surprisingly, we find that when $|\omega_x - \omega_y| \sim 0$ cooling becomes again ineffective. The optimal frequency difference for efficient 2D cooling is near the midpoint value – when $|\omega_x - \omega_y| \sim \frac{\kappa}{2}$ with the detuning set to $-\Delta \sim (\omega_x + \omega_y)/2$ (see Fig. 4).

We can understand qualitatively the reason for the optimal frequency difference $|\omega_x - \omega_y| \sim \frac{\kappa}{2}$ by calculating 2D optomechanical cooling formula:

$$\Gamma_{\text{opt},j} \equiv \text{Im} \left[\frac{2ig_j^2 \eta(\omega_j)}{1 - 2ig_k^2 \chi_k(\omega_j) \eta(\omega_j)} \right], \quad (23)$$

where $j = x, k = y$ or $j = y, k = x$ (from Eqs. (14)-(17) one readily finds the optomechanical cooling formula by calculating the imaginary part of the self-energy [27, 35]). Let us consider some special cases. Suppose first that $g_k \sim 0$ such that we have $\Gamma_{\text{opt},j} \sim \text{Im} [2ig_j^2 \eta(\omega_j)]$ – the latter is the usual optomechanical cooling rate which further reduces to $\Gamma_{\text{opt},j} \sim 4g_j^2/\kappa$. The numerator can be thus associated with the cooling rate from standard 1D cavity optomechanics. On the other hand the denominator depends only on the coupling to the other degree of freedom, $\sim g_k$, and is thus a genuinely 2D effect affecting the j -motion.

We are primarily interested in the configuration where both $\Gamma_{\text{opt},x}$ and $\Gamma_{\text{opt},y}$ are large. Let us start by considering the perfectly degenerate case, $\omega_x = \omega_y = -\Delta$ with $g = g_x \sim g_y$. Assuming the regime of strong cooperativity we find that the optomechanical rate reduces to the simple expression $\Gamma_{\text{opt},j} \sim \gamma$. The gas damping, γ , is tiny at the relevant pressures, and thus we are left only with a negligible optomechanical cooling rate – here γ arises from the denominator in Eq. (23), i.e. from the mechanical susceptibility $\chi_k(\omega_j)$ defined in Eq. (19), and thus the strong suppression of the optomechanical cooling rate is to be identified as a 2D effect. Loosely speaking, the energy that is extracted from the x -motion (y -motion) is immediately fed back to the y -motion (x -motion) with the optical field mediating this transition. In order to achieve any 2D cooling we thus require some degree of asymmetry, $\omega_x \neq \omega_y$, in order to disrupt the near-perfect exchange of energy between \hat{x} and \hat{y} via the optical field, and allow the latter to instead carry the energy away from the system.

We finally note that lowering the finesse does not necessarily improve 2D cooling. This is captured by the optomechanical cooling formula in Eq. (23) through the optical susceptibility η defined in Eq. (20): on the one hand, when we decrease the value of κ we enhance the 1D cooling channel (numerator), but, on the other hand, we also amplify the 2D heating channel (denominator).

B. Optimal particle size

For concreteness we will consider the parameters from [17] (but now with $\theta = \pi/4$) which is close to the optimal

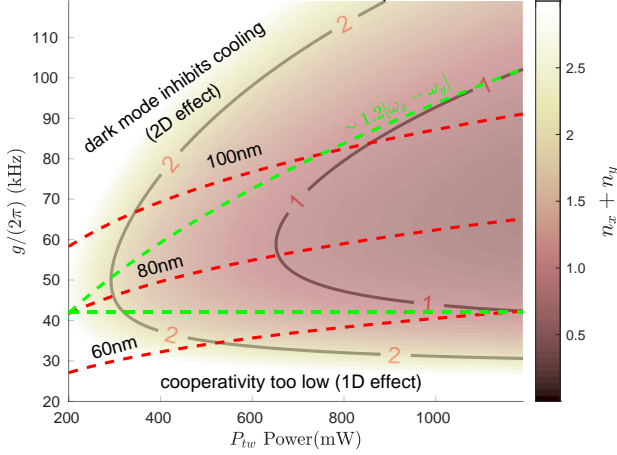


Figure 5. Numerical simulation of 2D phonon occupancy as a function of input power (P_{tw}) and mean optomechanical coupling ($g \equiv (g_x + g_y)/2$). The values are set as in [17] but $\theta = \pi/4$ and variable power and particle radius (which sets the optomechanical couplings). Cooling becomes ineffective if the cooperativity is too low (lower part of the figure) as well as if decoupled dark modes are formed (upper part of figure). Cooling to the 2D motional ground state, $n_x + n_y < 1$, is feasible already for a $\sim 80\text{nm}$ particle at $P_{\text{tw}} \sim 700\text{mW}$.

regime $|\omega_x - \omega_y| \lesssim \frac{\kappa}{2}$ (see Sec. V A), with the detuning set to $-\Delta \sim (\omega_x + \omega_y)/2$. For a given experimental implementation there are two key parameters that can be readily changed: the tweezer power, P , and particle radius, R . We express the relevant parameters for 2D cooling, $\omega_x, \omega_y, g_x, g_y$ as a function of the former. On one hand, we find that if the particle size is small ($\lesssim 60\text{nm}$) the cooperativity remains too low and one is limited to values above $n_x + n_y \sim 1$ – this is analogous to the requirement for 1D ground state cooling. On the other hand, if the particle size becomes large ($\gtrsim 100\text{nm}$) then cooling becomes again ineffective when $g_x, g_y \gtrsim |\omega_x - \omega_y|$. We find that there is a “Goldilocks zone” with the optimal particle size $\sim 80\text{nm}$ (see Fig. 5).

We can understand qualitatively the reason for the optimal particle size by looking again at the 2D optomechanical cooling formula in Eq. (23). We first note that $g_j \propto R^{3/2}$ where R is the nanoparticle radius, and that $g_j \propto P^{1/4}$ where P is the tweezer power, i.e. $g_j \propto R^{3/2} P^{1/4}$. For small (large) values of g_j the numerator (denominator) in Eq. (23) is small (large) and cooling becomes inhibited – this illustrates how the “Goldilocks zone” emerges from the competition of 1D effect in the numerator with the 2D effect in the denominator. In particular, the condition $g_j \lesssim |\omega_x - \omega_y|$ emerges from the denominator in Eq. (23) – we have $\chi_k(\omega_j) \sim |\omega_x - \omega_y|^{-1}$ as well as $\eta(\omega_j) \sim |\omega_x - \omega_y|^{-1}$ (since $-\Delta \sim (\omega_x + \omega_y)/2$) – and hence the denominator remains suppressed if $|g_k| \lesssim |\omega_x - \omega_y|$, i.e. cooling is not inhibited by the 2D hybridization effect.

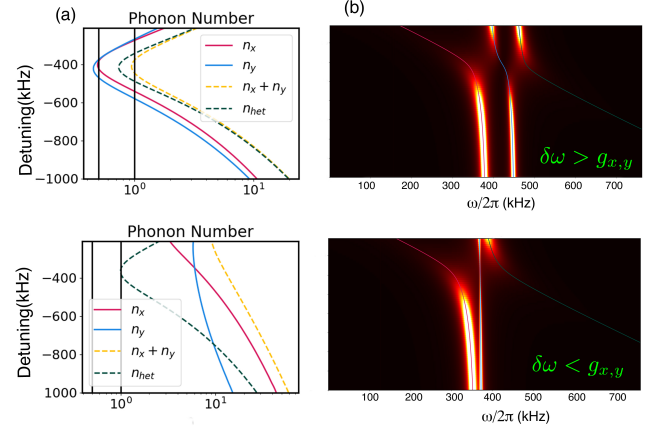


Figure 6. (a) Compares phonon occupancies for an elliptical trap used in the quantum cooling experiments [17], $\delta\omega = |\omega_x - \omega_y| > g_x \sim g_y$ (upper) with occupancies for a near-circular trap with the same parameters but $\delta\omega$ smaller so that $|\omega_x - \omega_y| < g_x \sim g_y$ (lower). The elliptical trap allows for 2D ground state cooling and the rescaled heterodyne follows occupancies closely, facilitating thermometry. For the near-circular trap, the modes remain hot and it is difficult to extract occupancies from the optical detection by the usual methods. The particle is positioned at a node (intensity minimum), $\theta_{\text{tw}} = \pi/4$, $R = 80\text{nm}$, input power $P_{\text{in}} = 0.8\text{W}$, and $\kappa = 193\text{kHz}$. (b) Corresponding heterodyne PSDs, with the classical modes overlaid. For the elliptical trap in the upper panels when the detuning is set to $-\Delta = 400$ kHz the modes are cooled to $n_x + n_y < 1$ and a dark region is seen at the centre of the crossing.

C. Reliable thermometry

In the previous sections we have shown that there exists an optimal experimental configuration (Sec. V A) and particle size (Sec. V A) to achieve simultaneous cooling of both x and y motions. However, inferring phonon occupancies from optically detected spectra in the presence of hybridisation is not straightforward. Here we show that the same experimental configuration that allows for optimal 2D cooling also allows for reliable thermometry.

Experiments exploiting heterodyne detection have access only to the optical field, $\hat{a} = \frac{1}{2}(\hat{Z}_L + i\hat{P}_L)$, from which one then extracts the the mechanical displacement spectra. In particular, the heterodyne PSD is given by [34]

$$S_{\text{het}}(\omega) \equiv S_{a_{\text{out}} a_{\text{out}}^\dagger}(\Delta_{\text{LO}} + \omega) + S_{a_{\text{out}}^\dagger a_{\text{out}}}(\Delta_{\text{LO}} - \omega), \quad (24)$$

where Δ_{LO} is the detuning of the local oscillator, and $\hat{a}_{\text{out}} = \hat{a} + \sqrt{\kappa}\hat{a}_{\text{in}}$ is the output field. In general, extracting the displacement spectra, $S_{xx}(\omega)$ and $S_{yy}(\omega)$, from the experimental heterodyne spectra, $S_{\text{het}}(\omega)$, is not straightforward. However, in the optimal case for 2D cooling (see Sec. V A) – when $g_x \simeq g_y \simeq g$ – one finds a simple relation between the intracavity field and the mechanical motions:

$$\hat{a}(\omega) \simeq \eta(\omega)g[\hat{x}^{3D}(\omega) + \hat{y}^{3D}(\omega)]. \quad (25)$$

Combining Eqs. (24)-(25) one then readily finds:

$$\frac{S_{\text{het}}(\omega)}{|\eta(\omega)|^2 g^2} \simeq S_{xx}(\omega) + S_{yy}(\omega), \quad (26)$$

which can be seen as the 2D extension of the familiar textbook relation arising in the 1D case.

We test Eq. (26) in Fig. 6: in panels (a) we compare the extracted phonon occupancies (using the heterodyne spectra) with the actual ones, and in panels (b) we show the PSDs for the heterodyne signal with the classical modes overlaid. The upper panels show the result for an elliptical trap lie within the ‘‘Goldilocks zone’’ where frequencies are sufficiently far apart so that both modes are in the quantum regime and moreover, the phonon occupancies inferred from rescaled heterodyne PSD agree reasonably well with those obtained from integrating $S_{xx}(\omega) + S_{yy}(\omega)$, in contrast with the near-circular trap, which lies outside this zone. In the latter case (near-circular trap) the modes remain hot and more complicated methods would be required to infer mode occupancies from the optically detected signal.

D. Understanding 2D cooling in terms of geometric bright/dark modes

We can gain further intuitive understanding of 2D cooling by considering a rotated reference frame – the cavity-based reference frame introduced in Fig. 1. We transform to the latter reference frame $(x^{(c)}, y^{(c)})$ by applying a rotation of angle θ :

$$\begin{bmatrix} x^{(c)} \\ y^{(c)} \end{bmatrix} = \begin{bmatrix} \sin\theta & \cos\theta \\ -\cos\theta & \sin\theta \end{bmatrix} \begin{bmatrix} x \\ y \end{bmatrix}. \quad (27)$$

The rotation in Eq. (27) in term induces a transformation of the modes: \hat{x}_b (\hat{x}_d) is the mode along (orthogonal to) the cavity axis. The Hamiltonian from Eq. ((3)) becomes

$$\frac{\hat{V}_{\text{int}}}{\hbar} = g_{bd}\hat{x}_b\hat{x}_d + g_b\hat{x}_b\hat{Z}_L. \quad (28)$$

We note that only \hat{x}_b is coupled to the light field while \hat{x}_d is completely decoupled – we will refer to them as bright and dark mode, respectively. The couplings are given by

$$g_{bd} = \frac{g_x g_y (\omega_y^2 - \omega_x^2)}{2(g_x^2 \omega_x + g_y^2 \omega_y)} \sqrt{\frac{\omega_x \omega_y}{\omega_{bd}^2}}, \quad (29)$$

$$g_b = \sqrt{\frac{g_x^2 \omega_x}{\omega_{bd}} + \frac{g_y^2 \omega_y}{\omega_{bd}}}, \quad (30)$$

where $\omega_{bd} = \sqrt{(\omega_x^2 + \omega_y^2)}/2$ is the weighted average of the original frequencies. We can further approximate the expressions by assuming $|\omega_x - \omega_y| \ll \omega_x, \omega_y$ whilst still

retaining the lowest order terms proportional to $\omega_y - \omega_x$. From Eqs. (29) and (30) we readily find

$$g_{bd} \approx \frac{g_x g_y (\omega_y - \omega_x)}{(g_x^2 + g_y^2)}, \quad (31)$$

$$g_b \approx \sqrt{g_x^2 + g_y^2}. \quad (32)$$

Eqs. (31) and (32) are the standard definitions of the bright/dark modes which are obtained by a rotation the abstract canonical space [28]. The latter differ from the geometric bright/dark modes induced by the physical rotation, but the two are however closely related and approximately coincide for small frequency differences.

The dark mode, \hat{x}_d , is by definition decoupled from the cavity mode and cannot be directly accessed – any cooling mechanism must rely on the coupling g_{bd} to the bright mode (the latter can then be controlled through the coupling g_b to the light). In other words, we have only the option to *sympathetically* cool the dark mode through the bright one. We see from Eq. (31) that the coupling g_{bd} depends on $|\omega_x - \omega_y|$: only when $|\omega_x - \omega_y|$ is large we can expect to *sympathetically* cool the dark mode through the bright one, but when $\omega_x = \omega_y$ the dark mode becomes completely inaccessible. However, if $|\omega_x - \omega_y|$ is large, then the cooling will become ineffective as the bright and dark mode will become effectively decoupled (the susceptibilities functions will act as filter to attenuate the sympathetic cooling channel). We thus have a ‘‘Goldilocks zone’’ in an intermediate range of $|\omega_x - \omega_y|$ values as we have already seen in the previous sections.

The emergence of the ‘‘Goldilocks zone’’ can be also understood from the 2D optomechanical cooling formulae (see Appendix (C) for a sketch of the derivation):

$$\Gamma_{\text{opt,b}} \sim \frac{4g_b^2}{\kappa}, \quad \Gamma_{\text{opt,d}} \sim \frac{g_{bd}^2 \kappa}{g_b^2}. \quad (33)$$

In order to cool effectively in 2D both $\Gamma_{\text{opt,b}}$ and $\Gamma_{\text{opt,d}}$ have to be larger than a certain minimum threshold value, $\Gamma_{\text{opt,b,d}} > \Gamma_{\text{min}}$ – these two conditions give rise to the Goldilocks zone. To gain further insight we write the coupling as $g \equiv g_x \sim g_y$ – we find $g_b \sim \sqrt{2}g$ and $g_{bd} \sim (\omega_y - \omega_x)/2$ – which further reduces the 2D optomechanical formulae to $\Gamma_{\text{opt,b}} \sim \frac{8g^2}{\kappa}$ and $\Gamma_{\text{opt,d}} \sim \frac{\kappa}{8g^2}(\omega_y - \omega_x)^2 \sim (\omega_y - \omega_x)^2/\Gamma_{\text{opt,b}}$. The two cooling rates become equal when $\Gamma_{\text{opt,b}} = \Gamma_{\text{opt,d}} = |\omega_y - \omega_x|$.

VI. DISCUSSION

We have investigated optomechanical interaction via coherent scattering of the nanoparticle motion in the tweezer transverse (x-y) plane with an optical cavity. We show that efficient cooling of the x and y motion to their quantum ground state requires a precise relation between

the difference of mechanical frequencies $|\omega_x - \omega_y|$, cavity decay rate κ and coupling rates g_x and g_y . We show that cooling and standard thermometry are efficient for a sufficiently elliptical optical trap, while for a more spherical trap the cooling will be hindered by strong three-way mode hybridization with the cavity mode. We find the optimal particle size that satisfies the conditions, thus allowing for 2D ground state cooling in the current experimental setup.

Free-fall experiments that propose recycling of particles – where particles would be trapped again after a sufficiently long free-fall time – require the nanoparticle energy to be low in all three translational motions. The motion along the optical tweezer axis can be cooled to its ground state via feedback cooling [26], thus extending our 2D scheme to fully prepare nanoparticles for free-fall experiments. In addition, the uncoupled three degrees of freedom can be used as a (quantum) sensor of forces acting along a specific direction, such as terrestrial gravity fluctuations [36].

ACKNOWLEDGMENTS

This work was presented at the ICTP online workshop Frontiers of Nanomechanics (September 2020). We are extremely grateful to Vladan Vuletić for insightful discussions about bright/dark modes. MT and TM acknowledge support from EPSRC grant EP/N031105/1. FH acknowledges an EPSRC studentship.

Appendix A: Notes on scattering force

In this appendix we look at the modification of the optomechanical interaction due to the shifted equilibrium position of the nanoparticle along the z-axis (with respect to the tweezer trap center). In particular, such a shifted equilibrium arises from the scattering radiation pressure force as we increase the particle size. We first find the new equilibrium position (Sec. A 1) and then calculate the new optomechanical couplings (Sec. A 2). We finally show that by using appropriately rotated optical quadratures the optomechanical formulae derived for the case of negligible scattering force – appropriate for small nanoparticles – extend also to the case with a shifted equilibrium position (Sec. A 3).

1. z-axis equilibrium position

The competition between the gradient force, F_{grad} , and the scattering force, F_{scatt} , modifies the nanoparticle's equilibrium position, z_0 , along the z-axis (the tweezer symmetry axis). In particular, the gradient and scattering force are given by [37]:

$$F_{\text{grad}} = -\frac{2\pi r^3}{c} \frac{\epsilon_R - 1}{\epsilon_R + 2} \partial_z I, \quad (\text{A1})$$

$$F_{\text{scatt}} = \frac{8\pi k^4 r^6}{3c} \left(\frac{\epsilon_R - 1}{\epsilon_R + 2} \right)^2 I, \quad (\text{A2})$$

respectively, where ϵ_R is the relative dielectric permittivity, c is the speed of light, $k = \frac{2\pi}{\lambda}$, λ is the wavelength, r is the particle radius, $I = P_{\text{tw}}/(\pi w_x w_y)$ (P_{tw}) is the laser intensity (power) at the center of the trap, and w_x , w_y are the beam waists. We readily find the equilibrium position, z_0 , from the condition $F_{\text{grad}} + F_{\text{scatt}} = 0$. Assuming $z_0/z_r \ll 1$, where $z_r = \pi w_x w_y/\lambda$ is the Rayleigh range, we find a simple result:

$$z_0 = \frac{\epsilon_R - 1}{\epsilon_R + 2} \frac{2k^4 z_R^2}{3} r^3, \quad (\text{A3})$$

but can otherwise numerically solve for the equilibrium position. Importantly, the larger the particle radius, r , the more the equilibrium position, z_0 , is displaced from the Gaussian beam focus [38].

2. Optomechanical couplings

We start from the coherent scattering interaction potential [18]:

$$\frac{\hat{V}_{\text{int}}}{\hbar} = E_d \cos[\phi + k(\hat{x} \sin(\theta) + \hat{y} \cos(\theta))] [\hat{a} e^{-i\xi} + \hat{a}^\dagger e^{i\xi}], \quad (\text{A4})$$

where $\xi = kz + \Phi(z)$, and $\Phi(z) = -\arctan(z/z_R)$ is the Gouy phase. The equilibrium position of the nanoparticle with respect to the tweezer trap center will be denoted by (x_0, y_0, z_0) , where we assume $x_0 = y_0 = 0$, while z_0 is given by Eq. A3 (for $z_0/z_r \ll 1$) or obtained by solving numerically for the equilibrium position.

Expanding the interaction potential in Eq. (A4) to quadratic order we find the following couplings:

$$\begin{aligned} \frac{\hat{V}_{\text{int}}}{\hbar} = & -g_{xY}^\xi \hat{x} \hat{Y} - g_{xP}^\xi \hat{x} \hat{P} - g_{yY}^\xi \hat{y} \hat{Y} - g_{yP}^\xi \hat{y} \hat{P} - g_{zY}^\xi \hat{z} \hat{Y} \\ & - g_{zP}^\xi \hat{z} \hat{P} - g_{xy}^\xi \hat{x} \hat{y} - g_{xz}^\xi \hat{x} \hat{z} - g_{yz}^\xi \hat{y} \hat{z}. \end{aligned} \quad (\text{A5})$$

Assuming $kz_R \gg 1$, neglecting terms of order $\mathcal{O}(z_0/z_R)$, while still retaining the phase $\xi \sim kz_0$, we find simple couplings

$$g_{xY}^\xi = g_{xY} \cos(\xi), \quad g_{xP}^\xi = g_{xY} \sin(\xi), \quad (\text{A6})$$

$$g_{yY}^\xi = g_{yY} \cos(\xi), \quad g_{yP}^\xi = g_{yY} \sin(\xi), \quad (\text{A7})$$

$$g_{xy}^\xi = \frac{g_{xy}}{Y_0} (Y_0 \cos(\xi) + P_0 \sin(\xi)). \quad (\text{A8})$$

where

$$g_{xY} = -E_d k \sin(\theta) \sin(\phi) x_{z\text{p}f}, \quad (\text{A9})$$

$$g_{yY} = -E_d k \cos(\theta) \sin(\phi) y_{z\text{p}f}, \quad (\text{A10})$$

$$g_{xy} = -E_d k^2 Y_0 \sin(\theta) \cos(\theta) \cos(\phi) x_{z\text{p}f} y_{z\text{p}f}. \quad (\text{A11})$$

For completeness we list also the z-couplings:

$$g_{zY}^\xi = g_{zP} \sin(\xi), \quad g_{zP}^\xi = g_{zP} \cos(\xi), \quad (\text{A12})$$

$$g_{xz}^\xi = \frac{g_{xz}}{P_0} [P_0 \cos(\xi) + Y_0 \sin(\xi)], \quad (\text{A13})$$

$$g_{yz}^\xi = \frac{g_{yz}}{P_0} [P_0 \cos(\xi) + Y_0 \sin(\xi)], \quad (\text{A14})$$

where

$$g_{zP} = E_d k \cos(\phi) z_{z\text{p}f}, \quad (\text{A15})$$

$$g_{xz} = -E_d k^2 P_0 \sin(\theta) \sin(\phi) x_{z\text{p}f} z_{z\text{p}f}, \quad (\text{A16})$$

$$g_{yz} = -E_d k^2 P_0 \cos(\theta) \sin(\phi) y_{z\text{p}f} z_{z\text{p}f}. \quad (\text{A17})$$

The couplings $g_{xY}, g_{yY}, g_{xy}, g_{zP}, g_{xz}, g_{yz}$ have been previously obtained by neglecting the scattering force and are valid for small nanoparticles [27].

3. Rotated optical quadratures

It is instructive to compare the case with negligible scattering force (i.e., $z_0 = 0$ and $\xi = 0$) with the case of an arbitrary z-axis displacement from the tweezer trap center (i.e., $z_0 > 0$ and $\xi > 0$). In particular, we introduce the rotated optical quadratures:

$$\begin{bmatrix} \hat{Y}^\xi \\ \hat{P}^\xi \end{bmatrix} = \begin{bmatrix} \cos(\xi) & -\sin(\xi) \\ \sin(\xi) & \cos(\xi) \end{bmatrix} \begin{bmatrix} \hat{Y} \\ \hat{P} \end{bmatrix}, \quad (\text{A18})$$

where the angle of rotation is $\xi \sim k z_0$, and \hat{Y}^ξ, \hat{P}^ξ (\hat{Y}, \hat{P}) denote the optical quadratures in the case with (without) the z_0 displacement.

Let us first consider the mean values. From Eq. (A5), writing the corresponding classical equations of motion, we find that the mean-value of the optical quadratures are given by

$$Y_0^\xi = -\frac{E_d \cos(\phi)}{\Delta^2 + (\frac{\kappa}{2})^2} [2\Delta \cos(\xi) - \kappa \sin(\xi)], \quad (\text{A19})$$

$$P_0^\xi = -\frac{E_d \cos(\phi)}{\Delta^2 + (\frac{\kappa}{2})^2} [2\Delta \sin(\xi) + \kappa \cos(\xi)]. \quad (\text{A20})$$

where Δ is the detuning, and κ the cavity decay rate. If we set $z_0 = 0$ (and hence $\xi = 0$) we find the simplified expression for the amplitude and phase quadratures, which we denote by Y_0 and P_0 , respectively. From Eqs. (A19)

and (A20) we readily see that Y_0^ξ, P_0^ξ and Y_0, P_0 are related by the rotation introduced in Eq. (A18).

Using now the rotated quadratures, \hat{Y}^ξ, \hat{P}^ξ , and the rotated mean values, Y_0^ξ, P_0^ξ , the interaction potential in Eq. (A5) reduces to the expression:

$$\begin{aligned} \frac{\hat{V}_{\text{int}}}{\hbar} = & -g_{xY} \hat{x} \hat{Y}^\xi - g_{yY} \hat{y} \hat{Y}^\xi - g_{zP} \hat{p} \hat{P}^\xi \\ & - g_{xy}^\xi \hat{x} \hat{y} - g_{xz}^\xi \hat{x} \hat{z} - g_{yz}^\xi \hat{y} \hat{z}, \end{aligned} \quad (\text{A21})$$

where

$$g_{xy}^\xi = -E_d k^2 Y_0^\xi \sin(\theta) \cos(\theta) \cos(\phi) x_{z\text{p}f} y_{z\text{p}f}, \quad (\text{A22})$$

$$g_{xz}^\xi = -E_d k^2 P_0^\xi \sin(\theta) \sin(\phi) x_{z\text{p}f} z_{z\text{p}f}, \quad (\text{A23})$$

$$g_{yz}^\xi = -E_d k^2 P_0^\xi \cos(\theta) \sin(\phi) y_{z\text{p}f} z_{z\text{p}f}. \quad (\text{A24})$$

We note that the potential in Eq. (A21) has the same form of the potential previously obtained for the case of small nanoparticles [27] (i.e. where one can neglect the displacement, z_0 , due to the scattering force): one formally replaces $\hat{Y} \rightarrow \hat{Y}^\xi$ and $\hat{P} \rightarrow \hat{P}^\xi$. Thus all the formulae obtained in [27] remain valid also when we consider a significant non-zero displacement along the z-axis (displacement from the tweezer trap center), provided we use the rotated mean values, Y_0^ξ and P_0^ξ , given in Eqs. (A19) and (A20), respectively.

For the special case considered in the main text the interaction potential remains of the same form as in the case without any z-axis displacement:

$$\frac{\hat{V}_{\text{int}}}{\hbar} = -g_x \hat{x} \hat{Z}_L - g_y \hat{y} \hat{Z}_L, \quad (\text{A25})$$

where we have defined $\hat{Z}_L \equiv \hat{Y}^\xi$, $g_x \equiv g_{xY}$, and $g_y \equiv g_{yY}$.

Appendix B: 2D phonon occupancy

A physical rotation acting on the adimensional operators has the form

$$\hat{v} \rightarrow \begin{bmatrix} R(\theta) & 0 \\ 0 & R(\theta) \end{bmatrix} \hat{v}, \quad (\text{B1})$$

where $\hat{v} = (\hat{x}, \hat{y}, \hat{p}_x, \hat{p}_y)^\top$. Following the conventions from [17, 18, 27] the rotation matrix is given by

$$R(\theta) = \begin{bmatrix} \sqrt{\frac{\omega_x}{\omega_{x'}}} \sin\theta & \sqrt{\frac{\omega_y}{\omega_{y'}}} \cos\theta \\ -\sqrt{\frac{\omega_x}{\omega_{y'}}} \cos\theta & \sqrt{\frac{\omega_y}{\omega_{x'}}} \sin\theta \end{bmatrix}, \quad (\text{B2})$$

where the primed (unprimed) frequencies denote original (transformed) quantities. To define an invariant measure

of 2D phonon occupancy, we should consider the transformation in physical space given by Eq. (B1) – this transformation maps the chosen initial reference frame to an arbitrary one. However, such a transformation will transform two decoupled harmonic oscillators in two coupled ones, which is not ideal to define the 2D phonon occupancy. This then suggests that tweezer reference frame – where the oscillators remain decoupled – is the most suitable frame to define the 2D mechanical phonon occupancy (the frame of normal mechanical modes).

Appendix C: 2D cooling formulae for bright/dark modes

In this section we derive the 2D optomechanical cooling rates for the dark/bright mode. We start from the Hamiltonian in Eq. (28) and write Hamilton's equation of motion:

$$\dot{\hat{x}}_b = \omega_b \hat{p}_b, \quad (\text{C1})$$

$$\dot{\hat{p}}_b = -\omega_b \hat{x}_b - 2g_{bd} \hat{x}_d - 2g_b \hat{Y}, \quad (\text{C2})$$

$$\dot{\hat{x}}_d = \omega_d \hat{p}_d, \quad (\text{C3})$$

$$\dot{\hat{p}}_d = -\omega_d \hat{x}_d - 2g_{db} \hat{x}_b, \quad (\text{C4})$$

$$\dot{\hat{Y}} = -\Delta \hat{P}, \quad (\text{C5})$$

$$\dot{\hat{P}} = \Delta \hat{Y} - 2g_b \hat{x}_b. \quad (\text{C6})$$

where we have introduced $g_{db} = g_{bd}$ to ease the reading of the equations.

In the following we will consider also non-conservative terms (damping and input noise) which we have previously omitted for clarity of presentation. We transform Eqs. (C3)-(C6) to second order differential equations by eliminating the momenta, and express the resulting equations in Fourier space:

$$\hat{x}_b(\omega) = J_{bd}(\omega) \hat{x}_d(\omega) + J_{bY}(\omega) \hat{Y}(\omega) + \tilde{x}_{b,\text{in}}(\omega), \quad (\text{C7})$$

$$\hat{x}_d(\omega) = J_{db}(\omega) \hat{x}_b(\omega) + \tilde{x}_{d,\text{in}}(\omega), \quad (\text{C8})$$

$$\hat{Y}(\omega) = J_{Yb}(\omega) \hat{x}_b(\omega) + \tilde{Y}_{\text{in}}(\omega), \quad (\text{C9})$$

which can be readily solved for $\hat{x}_b(\omega)$, $\hat{x}_d(\omega)$ and $\hat{Y}(\omega)$ (in terms of the input noises $\tilde{x}_{b,\text{in}}(\omega)$, $\tilde{x}_{d,\text{in}}(\omega)$ and $\tilde{Y}_{\text{in}}(\omega)$). The frequency dependent coupling coefficients are given by

$$J_{bd}(\omega) = 2g_{bd} \chi_b(\omega), \quad (\text{C10})$$

$$J_{db}(\omega) = 2g_{db} \chi_d(\omega), \quad (\text{C11})$$

$$J_{bY}(\omega) = 2g_b \chi_b(\omega), \quad (\text{C12})$$

$$J_{Yb}(\omega) = ig_b \eta(\omega), \quad (\text{C13})$$

where the susceptibilities are given by

$$\chi_{b,d}(\omega) = \frac{\omega_{b,d}}{-\omega^2 + \omega_{b,d}^2 - i\omega_j \gamma}, \quad (\text{C14})$$

$$\eta(\omega) = \frac{1}{-i(\omega + \Delta) + \frac{\kappa}{2}} - \frac{1}{i(-\omega + \Delta) + \frac{\kappa}{2}}. \quad (\text{C15})$$

To find the self-energy for the bright mode, \hat{x}_b , we need to solve (C8) and (C9) for $\hat{x}_d \equiv \hat{x}_d(\hat{x}_b)$ and $\hat{Y} \equiv \hat{Y}(\hat{x}_b)$ and insert the expression in Eq. (C7) for the bright mode. To find the self-energy for the dark mode, \hat{x}_d , we proceed in a completely analogous way – we solve (C7) and (C9) for $\hat{x}_b \equiv \hat{x}_b(\hat{x}_d)$ and $\hat{Y} \equiv \hat{Y}(\hat{x}_d)$ and insert the expression in Eq. (C8) for the bright mode. From the imaginary parts of the self-energies we can readily extract the optomechanical cooling rates:

$$\Gamma_{\text{opt},b} \equiv \text{Im} [2ig_b^2 \eta(\omega_b) + 4g_{bd}^2 \chi_d(\omega_b)] \approx \frac{4g_b^2}{\kappa}, \quad (\text{C16})$$

$$\Gamma_{\text{opt},d} \equiv \text{Im} \left[\frac{4g_{bd}^2 \chi_b(\omega_d)}{1 - 2ig_b^2 \chi_b(\omega_d) \eta(\omega_d)} \right] \approx \frac{g_{bd}^2 \kappa}{g_b^2}. \quad (\text{C17})$$

-
- [1] AA Michelson and EW Morley. On the relative motion of the earth and of the luminiferous ether. *Sidereal Messenger*, vol. 6, pp. 306-310, 6:306–310, 1887.
- [2] BP Abbott, R Abbott, TD Abbott, MR Abernathy, F Acernese, K Ackley, C Adams, T Adams, P Addesso, RX Adhikari, et al. Observation of gravitational waves from a binary black hole merger. *Physical review letters*, 116(6):061102, 2016.
- [3] Markus Aspelmeyer, Tobias J Kippenberg, and Florian Marquardt. Cavity optomechanics. *Reviews of Modern Physics*, 86(4):1391, 2014.
- [4] S Bose, K Jacobs, and PL Knight. Preparation of non-classical states in cavities with a moving mirror. *Physical Review A*, 56(5):4175, 1997.
- [5] James Millen, Tania S Monteiro, Robert Pettit, and A Nick Vamivakas. Optomechanics with levitated particles. *Reports on Progress in Physics*, 83(2):026401, 2020.
- [6] PF Barker and MN Snieder. Cavity cooling of an optically trapped nanoparticle. *Physical Review A*, 81(2):023826, 2010.
- [7] Darrick E Chang, CA Regal, SB Papp, DJ Wilson, J Ye, O Painter, H Jeff Kimble, and P Zoller. Cavity opto-mechanics using an optically levitated nanosphere. *Proceedings of the National Academy of Sciences*, 107(3):1005–1010, 2010.
- [8] GAT Pender, PF Barker, Florian Marquardt, James Millen, and TS Monteiro. Optomechanical cooling of levitated spheres with doubly resonant fields. *Physical*

- Review A*, 85(2):021802, 2012.
- [9] TS Monteiro, J Millen, GAT Pender, Florian Marquardt, D Chang, and PF Barker. Dynamics of levitated nanospheres: towards the strong coupling regime. *New Journal of Physics*, 15(1):015001, 2013.
- [10] Nikolai Kiesel, Florian Blaser, Uroš Delić, David Grass, Rainer Kaltenbaek, and Markus Aspelmeyer. Cavity cooling of an optically levitated submicron particle. *Proceedings of the National Academy of Sciences*, 110(35):14180–14185, 2013.
- [11] Peter Asenbaum, Stefan Kuhn, Stefan Nimmrichter, Ugur Sezer, and Markus Arndt. Cavity cooling of free silicon nanoparticles in high vacuum. *Nature communications*, 4(1):1–7, 2013.
- [12] Oriol Romero-Isart, Mathieu L Juan, Romain Quidant, and J Ignacio Cirac. Toward quantum superposition of living organisms. *New Journal of Physics*, 12(3):033015, 2010.
- [13] Pau Mestres, Johann Berthelot, Marko Spasenović, Jan Gieseler, Lukas Novotny, and Romain Quidant. Cooling and manipulation of a levitated nanoparticle with an optical fiber trap. *Applied Physics Letters*, 107(15):151102, 2015.
- [14] J Millen, PZG Fonseca, T Mavrogordatos, TS Monteiro, and PF Barker. Cavity cooling a single charged levitated nanosphere. *Physical review letters*, 114(12):123602, 2015.
- [15] PZG Fonseca, EB Aranas, J Millen, TS Monteiro, and PF Barker. Nonlinear dynamics and strong cavity cooling of levitated nanoparticles. *Physical review letters*, 117(17):173602, 2016.
- [16] Lorenzo Magrini, Richard A Norte, Ralf Riedinger, Igor Marinković, David Grass, Uroš Delić, Simon Gröblacher, Sungkun Hong, and Markus Aspelmeyer. Near-field coupling of a levitated nanoparticle to a photonic crystal cavity. *Optica*, 5(12):1597–1602, 2018.
- [17] U Delić, M Reisenbauer, K Dare, D Grass, V Vuletić, N Kiesel, and M Aspelmeyer. Cooling of a levitated nanoparticle to the motional quantum ground state. *Science*, 367(6480):892–895, 2020.
- [18] U Delić, M Reisenbauer, D Grass, N Kiesel, V Vuletić, and M Aspelmeyer. Cavity cooling of a levitated nanosphere by coherent scattering. *Physical review letters*, 122(12):123602, 2019.
- [19] Dominik Windey, Carlos Gonzalez-Ballester, Patrick Maurer, Lukas Novotny, Oriol Romero-Isart, and René Reimann. Cavity-based 3d cooling of a levitated nanoparticle via coherent scattering. *Physical review letters*, 122(12):123601, 2019.
- [20] Vladan Vuletić and Steven Chu. Laser cooling of atoms, ions, or molecules by coherent scattering. *Physical Review Letters*, 84(17):3787, 2000.
- [21] Vladan Vuletić, Hilton W Chan, and Adam T Black. Three-dimensional cavity doppler cooling and cavity sideband cooling by coherent scattering. *Physical Review A*, 64(3):033405, 2001.
- [22] Peter Domokos and Helmut Ritsch. Collective cooling and self-organization of atoms in a cavity. *Physical review letters*, 89(25):253003, 2002.
- [23] David R Leibbrandt, Jaroslaw Labaziewicz, Vladan Vuletić, and Isaac L Chuang. Cavity sideband cooling of a single trapped ion. *Physical review letters*, 103(10):103001, 2009.
- [24] Mahdi Hosseini, Yiheng Duan, Kristin M Beck, Yu-Ting Chen, and Vladan Vuletić. Cavity cooling of many atoms. *Physical review letters*, 118(18):183601, 2017.
- [25] Erik Hebestreit, Martin Frimmer, René Reimann, and Lukas Novotny. Sensing static forces with free-falling nanoparticles. *Physical review letters*, 121(6):063602, 2018.
- [26] Felix Tebbenjohanns, Martin Frimmer, Vijay Jain, Dominik Windey, and Lukas Novotny. Motional sideband asymmetry of a nanoparticle optically levitated in free space. *Physical Review Letters*, 124(1):013603, 2020.
- [27] M Toroš and TS Monteiro. Quantum sensing and cooling in three-dimensional levitated cavity optomechanics. *Physical Review Research*, 2(2):023228, 2020.
- [28] AB Shkarin, NE Flowers-Jacobs, SW Hoch, AD Kashkanova, C Deutsch, J Reichel, and JGE Harris. Optically mediated hybridization between two mechanical modes. *Physical review letters*, 112(1):013602, 2014.
- [29] W Neuhauser, M Hohenstatt, P Toschek, and H Dehmelt. Optical-sideband cooling of visible atom cloud confined in parabolic well. *Physical Review Letters*, 41(4):233, 1978.
- [30] Simon Gröblacher, Klemens Hammerer, Michael R Vanner, and Markus Aspelmeyer. Observation of strong coupling between a micromechanical resonator and an optical cavity field. *Nature*, 460(7256):724–727, 2009.
- [31] Andrés de los Ríos Sommer, Nadine Meyer, and Romain Quidant. Strong optomechanical coupling at room temperature by coherent scattering. *arXiv preprint arXiv:2005.10201*, 2020.
- [32] Vijay Jain, Jan Gieseler, Clemens Moritz, Christoph Delgado, Romain Quidant, and Lukas Novotny. Direct measurement of photon recoil from a levitated nanoparticle. *Physical review letters*, 116(24):243601, 2016.
- [33] T Seberson and F Robicheaux. Distribution of laser shot-noise energy delivered to a levitated nanoparticle. *Physical Review A*, 102(3):033505, 2020.
- [34] Warwick P Bowen and Gerard J Milburn. *Quantum optomechanics*. CRC press, 2015.
- [35] Florian Marquardt, Joe P Chen, Aashish A Clerk, and SM Girvin. Quantum theory of cavity-assisted sideband cooling of mechanical motion. *Physical review letters*, 99(9):093902, 2007.
- [36] Jan Harms. Terrestrial gravity fluctuations. *Living Reviews in Relativity*, 22(1):6, 2019.
- [37] Yasuhiro Harada and Toshimitsu Asakura. Radiation forces on a dielectric sphere in the rayleigh scattering regime. *Optics communications*, 124(5-6):529–541, 1996.
- [38] Chris Timberlake, Marko Toroš, David Hempston, George Winstone, Muddassar Rashid, and Hendrik Ulbricht. Static force characterization with fano anti-resonance in levitated optomechanics. *Applied Physics Letters*, 114(2):023104, 2019.